Remote Sensing of Environment 199 (2017) 350–359

Contents lists available at ScienceDirect

Remote Sensing of Environment

journal homepage: www.elsevier.com/locate/rse

Capturing species-level drought responses in a temperate deciduous forest using ratios of photochemical reflectance indices between sunlit and shaded canopies

Taehee Hwang[a,*,1], Hamed Gholizadeh[a,1], Daniel A. Sims[a,1], Kimberly A. Novick[b], Edward R. Brzostek[c,d], Richard P. Phillips[c], Daniel T. Roman[b,e], Scott M. Robeson[a], Abdullah F. Rahman[a,f]

[a] Department of Geography, Indiana University Bloomington, Bloomington, IN 47401, USA
[b] School of Public and Environmental Affairs, Indiana University Bloomington, Bloomington, IN 47401, USA
[c] Department of Biology, Indiana University Bloomington, Bloomington, IN 47401, USA
[d] Department of Biology, West Virginia University, Morgantown, WV 26506, USA
[e] U.S. Department of Agriculture, Forest Service, Northern Research Station, Grand Rapids, MN 55744, USA
[f] Coastal Studies Lab, University of Texas Rio Grande Valley, South Padre Island, TX 78597, USA

ARTICLE INFO

Keywords:
PRI
Isohydricity
Drought
LUE
Imaging spectroscopy
MODIS

ABSTRACT

To classify trees along a spectrum of isohydric to anisohydric behavior is a promising new framework for identifying tree species' sensitivities to drought stress, directly related to the vulnerability of carbon uptake of terrestrial ecosystems with increased hydroclimate variability. Trees with isohydric strategies regulate stomatal conductance to maintain stationary leaf water potential, while trees with anisohydric strategies allow leaf water potential to fall, which in the absence of significant hydraulic cavitation will facilitate greater rates of carbon uptake. Despite the recognition of the gas exchange consequences of isohydric and anisohydric strategies for individual tree species, there have been few studies regarding whether isohydric trees produces distinct spectral signatures under drought stress that can be remotely sensed. Here, we examined the capability of four vegetation indices (PRI, NDVI, $NDVI_{705}$, and EVI) to capture the differences in spectral responses between isohydric and anisohydric trees within a deciduous forest in central Indiana, USA. Both leaf-level spectral measurements and canopy-scale satellite observations were used to compare peak growing-season spectral signatures between a drought and a non-drought year. At the leaf scale, two vegetation indices (NDVI and $NDVI_{705}$) failed to capture the drought signal or the divergent isohydric/anisohydric behavior. EVI successfully captured the drought signal at both leaf and canopy scales, but failed to capture the divergent behavior between isohydric and anisohydric tree species during the drought. PRI captured both drought signals and divergent isohydric/anisohydric behavior at both leaf and canopy scales once normalized between sunlit (backward direction images) and shaded (forward direction images) portions of canopy, which indicates drought stress and subsequent photosynthetic down-regulation are greater in the sunlit portion of canopy. This study presents a significant step forward in our ability to directly mapping emergent isohydricity at different scales based on divergent spectral signatures between sunlit and shaded canopies.

1. Introduction

Recently, many forested regions in the United States have experienced increasing drought stress under ongoing climate change (Dai, 2013). Warmer temperatures have increased hydroclimate variability (Seager et al., 2009; O'Gorman and Schneider, 2009) with more frequent droughts, contributing to acute reductions in net ecosystem productivity (Roman et al., 2015), prolonged water stress (Brzostek et al., 2014; Xu and Baldocchi, 2003), and widespread tree mortality (Adams et al., 2009; Allen and Breshears, 2007; McDowell and Allen, 2015) in forested ecosystems. Differences between tree species in their response to imposed hydrologic stress can be evaluated by characterizing species along a continuum of isohydric to anisohydric behavior (Choat et al., 2012; Klein et al., 2014; Martinez-Vilalta et al., 2014).

* Corresponding author.
E-mail address: taehee@indiana.edu (T. Hwang).
[1] These three authors equally contributed to the paper.

http://dx.doi.org/10.1016/j.rse.2017.07.033
Received 13 December 2016; Received in revised form 11 July 2017; Accepted 28 July 2017
Available online 04 August 2017
0034-4257/

Despite the risk of xylem cavitation associated with highly negative leaf water potentials, trees with anisohydric strategies frequently sustain high stomatal conductance during drought (Matheny et al., 2017; Meinzer et al., 2017; Roman et al., 2015; Yi et al., 2017). In the absence of significant xylem cavitation, this strategy can also support relatively high levels of photosynthesis during periods of drought stress. In contrast, trees with isohydric strategies regulate stomatal conductance to maintain a relatively stationary leaf water potential as soil moisture declines. This strategy reduces embolism risk, but at a cost of reduced carbon assimilation (McDowell et al., 2008). The ratio of drought-driven declines in carbon uptake as compared to stomatal conductance depends on the plasticity of the plant's intrinsic water use efficiency, which can increase during periods of hydraulic stress, but not typically to an extent to completely mitigate losses in carbon uptake linked to stomatal closure (Novick et al., 2015). In relatively mesic forests like Eastern US, where drought events can have large effects on carbon and water cycling but rarely cause extensive hydraulic failure, the isohydric/anisohydric continuum is well suited for predicting the extent to which trees regulate their stomates during drought periods (Novick et al., 2015; Roman et al., 2015; Yi et al., 2017), as well as the resulting carbon assimilation strategies. The sensitivity of gross primary production (GPP) to drought stress has been shown to depend strongly on the relative proportion of isohydric vs. anisohydric tree species in forest stands (Roman et al., 2015). Recent works also suggest that isohydric stands are associated with greater interannual variability of evapotranspiration and reduced productivity compared to anisohydric stands, as related to strong isohydric behavior in their stomatal control and cavitation vulnerability (Ford et al., 2011; Novick et al., 2016; Stoy et al., 2006). As a result, the degree to which forest stands respond isohydrically or anisohydrically to drought stress directly influences ecosystem productivity and has the potential to cause cascading effects on regional carbon storage.

While diagnosing isohydric vs. anisohydric stomatal responses is relatively straightforward, albeit labor-intensive, at the tree level (Meinzer et al., 2016), we have little understanding of how this behavior can be detected at large scales using remote sensing data. Specifically, there has been limited research regarding whether isohydric and anisohydric trees possess distinct spectral responses under drought stress (Sims et al., 2014) that can be remotely sensed and mapped to parameterize large-scale GPP models (Konings and Gentine, 2016; Sperry et al., 2016). Classically, light use efficiency (LUE) based GPP models have been widely used to assess the impact of droughts on carbon sequestration at a global scale (e.g. Song et al., 2013). In these models, GPP is usually proportional to the multiplicative term between LUE and absorbed photosynthetically active radiation (APAR). However, remote sensing metrics of canopy greenness often fail to capture small changes in leaf area or its function (i.e. stomatal closure) that accompany drought (Asner et al., 2004; Hwang et al., 2008; Sims et al., 2014). For this reason, most remote-sensing based terrestrial productivity models use water stress functions that downregulate LUE values under conditions of low water availability, based on either vapor pressure deficit (VPD) or soil moisture metrics (Song et al., 2013). These models are often applied to a wide range of vegetation composition and formulate the stomatal responses with a single set of ecophysiological model parameters based on the major plant functional types (e.g. Biome Parameter Look-Up Table for MODIS GPP; Zhao et al., 2005). Consequently, current model structures cannot reproduce observed differences in drought sensitivity among isohydric and anisohydric species within temperate deciduous forests. This mismatch between our theoretical understanding of plant drought response and its representation in models highlights a critical knowledge gap in understanding the vulnerability of carbon sequestration of terrestrial ecosystems under increased hydroclimate variability, especially in terms of species-specific variability with different water use and carbon assimilation strategies under drought conditions.

Recently, there have been advances in directly mapping LUE using imaging spectroscopy from different platforms. LUE mapping using remote sensing data is mostly based on the detection of excess energy not used in photosynthesis especially under drought conditions (Coops et al., 2010; Demmig-Adams and Adams, 1996), using the photochemical reflectance index (PRI) (Gamon et al., 1992; Gamon et al., 1997; Penuelas et al., 1995). PRI has been successfully applied across various remote sensing platforms ranging from narrow bandwidth spectro-radiometers to the Moderate Resolution Imaging Spectroradiometer (MODIS) (Drolet et al., 2008; Drolet et al., 2005; Goerner et al., 2009). Although PRI values are closely related to photosynthetic LUE values across different scales (see Garbulsky et al., 2011), PRI-LUE relationships often show strong sensitivity to shadow fractions following sun-target-sensor geometry (Drolet et al., 2005; Hall et al., 2008; Hilker et al., 2008), as well as canopy structures and soil background reflectance (Barton and North, 2001; Suárez et al., 2008). Across forest ecosystems, the correlation between LUE and PRI for sunlit canopy is higher than shaded canopy during water-stress conditions (Hall et al., 2008; Zhang et al., 2016). Expanding on this framework, known correlations between view angle and canopy LUE suggest that the variability in PRI values with view angle is directly related to the degree of down-regulation between sunlit and shaded portions of the canopy (Coops et al., 2010; Drolet et al., 2005). Using multi-angle satellite systems, such as backward and forward direction images, to capture the sunlit and shaded portion of canopy, respectively (Hall et al., 2012; Hall et al., 2008), it may be possible to derive canopy responses to drought (i.e. isohydry vs. anisohydry) by quantifying the extent to which sunlit and shaded canopies differ in PRI.

In this paper, we hypothesize that the degree to which canopies downregulate photosynthesis under drought stress (isohydry vs. anisohydry) is directly correlated with the magnitude of the differences in PRI between sunlit and shaded portions of canopy (Coops et al., 2010). Further, using both leaf and canopy scale measurements, we seek (1) to capture the difference in leaf-scale spectral signatures between isohydric and anisohydric trees species under drought stress, and (2) to examine whether this behavior can be detected at the canopy scale using multi-angle MODIS images. To meet these objectives, we combined site-level spectral observations and remotely sensed data for a biologically diverse temperature deciduous forest that contains a broad spectrum of isohydric and anisohydric species, and that experienced an exceptionally severe drought in 2012 (Roman et al., 2015).

2. Methods and materials

2.1. Study area

The study site is located in the Morgan Monroe State Forest (MMSF; 39.3232°N, 86.4131°W) in central Indiana, USA. MMSF is a deciduous broadleaf forest with average canopy height and rooting depth of 27 m and 0.44 m, respectively (Ehman et al., 2002). Among the common tree species found in the study region, sugar maple (*Acer saccharum*), tulip poplar (*Liriodendron tulipifera*) and sassafras (*Sassafras albidum*) are generally recognized to be among the most isohydric (or conservative) species, whereas white and red oaks (*Quercus alba* and *Q. rubra*) are anisohydric (or non-conservative) (Choat et al., 2012; Novick et al., 2015; Roman et al., 2015). Based on measurements of trees with diameter at breast height ≥ 10 cm made in 54 large plots in March 2011, the study site is dominated by isohydric species such as sugar maple, tulip poplar and sassafras, which represent 21%, 25%, and 10% of total basal area, respectively, while the anisohydric white and red oaks represent 5% and 3%, respectively. The study site experienced a severe drought during the summer (June–August) of 2012. During this time period, the total rainfall was 135 mm, which is < 50% of average June–August rainfall (302 mm from 1999 to 2015 except for 2012) (Fig. S1; June and July rainfall was just ~10% of the long-term mean). As a result, there was a dramatic early dry down of soil water content in 2012 (Fig. 1). In field measurements and remote sensing analyses, we

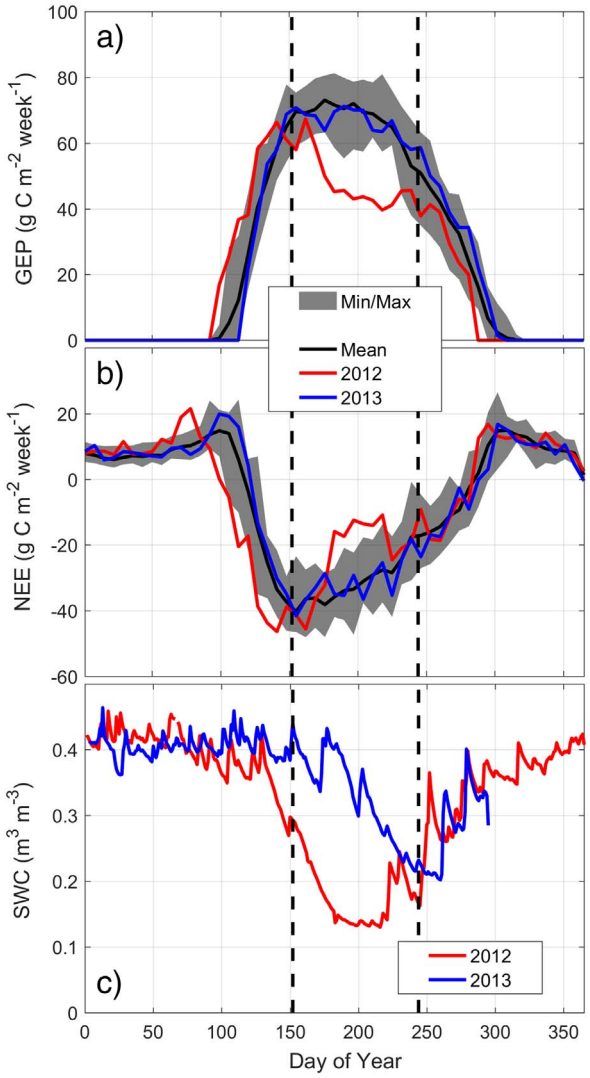

Fig. 1. Long-term tower-based measurements of (a) weekly gross ecosystem productivity (GEP), (b) weekly net ecosystem exchange (NEE), and (c) mean daily volumetric soil water content (SWC) at the Morgan-Monroe State Forest flux tower in the study site. The gray regions represent the minimum and maximum ranges from 1999 to 2015, except for 2012 (drought year). The vertical dashed lines show the peak growing season (June–August). Negative NEE values represent carbon sinks.

also include data from 2011 and 2013 to represent normal and wet years, respectively (Fig. S1).

2.2. Ecosystem measurements

The net ecosystem exchange of CO_2 (NEE) has been continuously measured from the MMSF *AmeriFlux* Tower (site code US-MMS) since 1998. Carbon dioxide and water vapor fluxes were measured at the top of the tower (i.e., $z = 46$ m) using a sonic anemometer (CSAT-3; Campbell Scientific Inc.) and a closed-path infrared gas analyzer (LI-7000; LI-COR, Lincoln, NE), which is calibrated weekly. Eddy covariance NEE data were recorded continuously at a frequency of 10 Hz, and filtered for periods of low turbulence (i.e. friction velocity < 0.3 m s^{-1}). Nocturnal and dormant season NEE data were then used parameterize a model for ecosystem respiration (RE), which was subtracted from NEE to derive an estimate of gross ecosystem productivity (GEP), as discussed in detail in Dragoni et al. (2011), Schmid et al. (2000), and Sulman et al. (2016).

Absorbed photosynthetically active radiation (APAR) values were estimated from the difference of PAR measurements between top and below the canopy. Total incoming photosynthetically active radiation (IPAR) values were measured at 46-m height using a quantum sensor (BF3, Delta-T Devices Ltd., Cambridge), while below-canopy PAR (PAR_{below}) values measured at 2-m height (Li-190, Li-COR, Lincoln, NE). Hourly albedo (α) values were estimated from shortwave incoming and reflected irradiance measurements from a net radiometer (CNR1, Kipp & Zonen, Netherlands), installed at 46-m height. Hourly absorbed photosynthetically active radiation (APAR) and fraction of absorbed PAR (FPAR) values were calculated as follows:

$$APAR = IPAR \cdot (1 - \alpha) - PAR_{below} \quad (1)$$

$$FPAR = APAR/IPAR \quad (2)$$

Hourly GEP and APAR estimates were used to calculate hourly LUE (= GEP/APAR) during the peak growing season (June through August) in 2011, 2012, and 2013, each representing normal, dry, and wet years, respectively. Weekly leaf area index (LAI) values have been measured along three transects ($n = 30$ total) around the flux tower at dawn (LAI-2200, Li-COR, Lincoln, NE) during the whole growing season (March–November). Volumetric soil water content (SWC) were also continuously measured from the top 30 cm soil layer by reflectometer probes (CS615 and CS616; Campbell Scientific, Logan, UT).

2.3. Leaf-scale spectroscopic and gas exchange measurements

Using a portable field spectroradiometer (UniSpec-SC Spectral Analysis System, PP Systems Inc., Amesbury, MA) and photosynthetic system (Li-6400Xt, Li-COR, Lincoln, NE), both leaf reflectance and photosynthesis were measured for the intact leaves around midday (10 am–3 pm) weekly from June through August in 2012 and 2013. We selected three trees with similar sizes from each species group: sugar maples (mean diameter at breast height: 44.1, 44.2, and 48.4 cm), tulip poplars (62.5, 62.8, and 86.7 cm), sassafras (41.4, 34.0, and 36.1 cm), and oaks (two white oaks: 39.2 and 43.8 cm, one red oak: 47.6 cm). Using a 25-m boom lift, five sunlit and five shaded leaves were selected for each tree from the top and bottom of the canopy, respectively. Both spectroscopic and gas exchange measurements were performed on the same leaves attached to the trees, but we did not measure the same leaves over the entire experiment. Leaf gas exchange measurement was performed over a short period of time (< 2 min) with chamber conditions (CO_2 concentration, temperature, humidity, and PAR) set to match ambient values (Roman et al., 2015). Previous analysis of the dynamics of leaf water potential (pre-dawn and midday), also collected concurrently with the gas exchange measurements, have been used to show that oaks behaved very anisohydrically during the 2012 drought, while other species were more isohydric (Roman et al., 2015). Leaf reflectance values were also measured at 3-nm intervals within the visible and near infrared electromagnetic spectrum (400–1000 nm), later interpolated to 1-nm intervals. All spectral and photosynthetic measurements were averaged separately for sunlit and shaded leaves of each tree. These concurrent measurements of leaf reflectance and photosynthesis provide a unique opportunity to test the ability to capture isohydric vs. anisohydric behavior during the severe drought using remote sensing data.

2.4. Leaf-scale spectral indices

In this study, we used four spectral indices based on narrow bands of the electromagnetic spectrum: photochemical reflectance index (PRI), normalized difference vegetation index (NDVI), red edge NDVI ($NDVI_{705}$), and enhanced vegetation index (EVI) at both leaf- and canopy-scale spectral measurements (Table 1). PRI directly quantifies the reflectance change associated with xanthophyll absorption (at 531 nm) (Penuelas et al., 1995) and the associated LUE response (Drolet et al., 2008; Drolet et al., 2005; Garbulsky et al., 2013; Rahman et al., 2004; Zhang et al., 2016). A simple transformation was applied to PRI values

Table 1
Four narrow-band spectral indices (PRI, NDVI, $NDVI_{705}$, and EVI) used in this study.

Spectral index	Equation	Reference
PRI or sPRI	$PRI = \frac{\rho_{531}-\rho_{570}}{\rho_{531}+\rho_{570}}$; $sPRI = \frac{PRI+1}{2}$	Gamon et al. (1992), Penuelas et al. (1995), Rahman et al. (2004)
NDVI	$NDVI = \frac{\rho_{858.5}-\rho_{645}}{\rho_{858.5}+\rho_{645}}$	Tucker (1979)
$NDVI_{705}$	$NDVI_{705} = \frac{\rho_{750}-\rho_{705}}{\rho_{750}+\rho_{705}}$	Sims and Gamon (2002)
EVI	$EVI = 2.5\frac{\rho_{858.5}-\rho_{645}}{\rho_{858.5}+6\rho_{645}-7.5\rho_{469}+1}$	Huete et al. (1997)

ρ_n is reflectance at n nm. PRI: photochemical reflectance index, NDVI: normalized difference vegetation index, $NDVI_{705}$: red edge NDVI, and EVI: enhanced vegetation index.

to avoid negative or near-zero values, known as scaled-PRI (sPRI; Table 1). For NDVI and EVI calculations, we used the reflectance of 645, 858.5, and 469 nm wavelengths, the middle of the MODIS band 1 (red), 2 (near infrared), and 3 (blue) to facilitate the comparison with MODIS vegetation indices. The red edge NDVI ($NDVI_{705}$) represents the normalized difference between the 705 and 750 nm wavelengths, developed based on the chlorophyll index (Sims and Gamon, 2002). While PRI captures drought-induced instantaneous physiological changes in the xanthophyll cycle, other leaf-scale indices were sensitive to chlorophyll-related changes during droughts (Marchin et al., 2010; Munne-Bosch et al., 2001). Additionally, the canopy-scale NDVI and EVI values also capture structural changes (e.g. LAI, leaf inclination angle etc.) accompanying droughts. We compared these four spectral indices and photosynthesis measurements during the peak drought period (July to August) in 2012 with the same period in a following wet year (2013). We examined the differences in the spectral indices in regards to the photosynthesis between dry and wet years, and between isohydric and anisohydric species both at the leaf and canopy scales. To capture the divergence in spectral indices between sunlit and shaded portions of canopy, we calculated the sunlit-to-shaded ratios in this study, such as $PRI_{sunlit}/PRI_{shaded}$. These ratio indices also make it possible to normalize seasonal changes of PRI, driven by the changes in leaf color and carotenoids-to-chlorophyll contents (Filella et al., 2009; Gamon et al., 2016; Wong and Gamon, 2015).

2.5. MODIS data processing

We extracted the 250-m MODIS NDVI and EVI data (MOD13Q1) around the flux tower from 2001 to 2014 using the MODIS Web Service Tool (https://modis.ornl.gov/data/modis_webservice.html). We used only the pixel values with a 'good' quality, based on the Pixel Reliability parameter (Didan and Huete, 2006). The NDVI and EVI results were presented by averaging a 3 × 2-km area around the flux tower, which represents relatively homogenous forest cover. We also calculated the canopy-scale sPRI values using MODIS Terra and Aqua data (collection 6) at the same spatial extent. Three MODIS products (MOD/MYD021KM, MOD/MYD03, and MOD/MYD35) were downloaded from the Level-1 and Atmosphere Archive and Distribution System (LAADS; https://ladsweb.nascom.nasa.gov/) for June, July, and August of 2011, 2012, and 2013. The MOD/MYD021KM product includes calibrated and geolocated at-aperture radiances at 1-km resolution for 36 MODIS bands. We only analyzed the pixels which centroids are located within the 3 × 2-km area in the sPRI calculation. Since the reference band used in PRI (i.e., the band at 570 nm) is not available in MODIS products, we applied a modified approach proposed by Drolet et al. (2005) to produce the reflectance data required to calculate sPRI.

While Drolet et al. (2005) used band 13 as the reference band, previous research at MMSF has shown that band 13 is likely saturated for terrestrial observations (Goerner et al., 2009). As a result, our calculation of PRI uses band 1 as the reference and band 11 as the detection band. Recently, this index was suggested to be renamed as a Chlorophyll/Carotenoid Index (CCI) to monitor evergreen photosynthetic activity (Gamon et al., 2016). Additionally, previous studies have shown that atmospheric correction of MODIS data does not improve the PRI results and it may even degrade the correlation between PRI and LUE (Goerner et al., 2011). So, instead of using atmospherically corrected reflectance values, we used the top-of-atmosphere (TOA) reflectance to calculate PRI (He et al., 2016). The MOD/MYD35 products were also used for cloud masking and removing cloud-covered pixels. We used only the pixels with the 'confident clear' quality flag in the MOD/MYD35 products. To remove pixels with large footprints, we eliminated all pixels with sensor zenith angle larger than 40°.

From the MODIS Terra and Aqua data, we calculated the PRI values for backward (sun is behind the sensor) and forward (sun is in front of the sensor) direction images which effectively capture the spectral signatures of sunlit and shaded portion of canopy, respectively. The solar/sensor azimuth and zenith angles and coordinates of all pixels from the MOD/MYD03 product were used to determine the backward and forward direction images. Using the solar and sensor azimuth angles obtained from MOD/MYD03 products, the relative azimuth angle Δ can be defined as follows:

$$\Delta = \begin{cases} |\theta - \theta_0| \ \ if\ 0^\circ \le |\theta - \theta_0| \le 180^\circ \\ 360^\circ - |\theta - \theta_0| \ if\ |\theta - \theta_0| > 180^\circ, \end{cases} \quad (3)$$

where θ and θ_0 are the sensor and solar azimuth angles, respectively. Backward direction images have a relative azimuth angle less than or equal to 60°, while forward direction images have a relative azimuth angle > 60° (Drolet et al., 2005). Note that the sunlit portion of canopy dominates the field of view of the sensor with smaller Δ angles (backward direction) with increasing the shaded portion with larger Δ angles (forward direction) (Cheng et al., 2012; Hall et al., 2008). In a manner similar to the leaf-scale sunlit-to-shaded sPRI ratios, the sPRI ratios were also calculated between backward and forward direction images. However, the MODIS PRI values are not essentially paired simply because cloud-free backward and forward images were not collected on the same days, different with the tree-level measurements. To avoid no PRI values in either backward or forward direction images at a short time interval, we calculated the PRI ratios over three-week intervals during the peak growing season (June–August) from 2011 to 2013.

2.6. Statistical analyses

We performed two-sample Welch's (unequal variances) *t*-tests with a null hypothesis that the group mean of 2012 (dry year) is greater than that of 2013 (wet year) during the peak drought period (July to August). We applied this test to all four spectral indices (PRI, NDVI, $NDVI_{705}$, and EVI; Table 1) and their ratios at the tree level, as well as to all pixel-level MODIS PRI values at the canopy scale. For three groups among normal (2011), dry, (2012), and wet (2013) years, we applied the analysis of variance (ANOVA) tests to evaluate whether the means of three groups are equal.

3. Results

3.1. Flux and gas exchange measurements

At the canopy scale, both GEP and NEE from the flux tower were reduced to an unprecedented level during the 2012 drought event (Fig. 1). During the peak drought period (July–August), the magnitudes of weekly GEP and NEE were over 30 g C m^{-2} (< 40% of mean value) and 20 g C m^{-2} lower (< 55% of mean value) respectively, compared to the baseline mean GEP and NEE (1999–2015 except for 2012). Significant differences in midday (10 am–3 pm) hourly APAR and GEP between 2012 and 2013 were also observed (Fig. 2). Mean APAR values

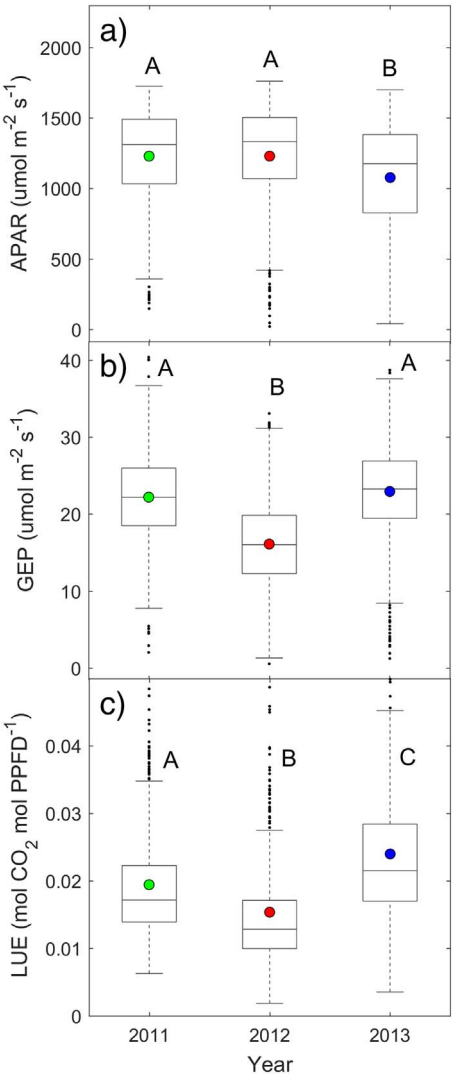

Fig. 2. Hourly midday (10 am–3 pm) (a) absorbed photosynthetically active radiation (APAR), (b) gross ecosystem productivity (GEP), and (c) light use efficiency (LUE) values from June through August in normal (2011 – green), drought (2012 – red), and wet year (2013 – blue) years from the Morgan Monroe State Forest flux tower. Circles are the mean values, while black dots are outliers. Different letters (A–C) denote significant differences in the group means using an analysis of variance (ANOVA) test ($p < 0.01$). (For interpretation of the references to color in this figure legend, the reader is referred to the web version of this article.)

were significantly higher ($p < 0.01$) in 2012 (dry) than in 2013 (wet), which were largely driven by significantly higher incoming PAR due to less frequent clouds with little changes in fraction of absorbed PAR (FPAR) (Fig. S2). As a result, mean hourly LUE (=GEP/APAR) values were significantly lower in 2012 than in 2013 ($p < 0.01$). It is worthwhile to note that LUE values in the normal year (2011) were between the values in wet and dry years.

Leaf gas exchange measurements showed similar significant decreases in mean net photosynthesis (PS) during the drought ($p < 0.001$), as well as divergent behavior between isohydric and anisohydric species (Fig. 3). In 2012, mean leaf PS values were reduced by about 30–50% compared to those in 2013 for the three isohydric species (sugar maple, tulip poplar, and sassafras). In the sunlit leaves, tulip poplar showed the largest percent decrease (41.6%) in the mean values, followed by sassafras (37.7%) and sugar maple (31.7%). In the shaded leaves, sassafras showed the largest percent decrease (46.2%), followed by sugar maple (40.9%) and tulip poplar (33.8%). Sunlit leaves usually had higher levels of PS than the shaded ones, and they showed larger decreases in the absolute magnitudes of PS during the 2012 drought. However, oaks (anisohydric) still maintained relatively high levels of PS both in sunlit and shaded leaves. While stomatal conductance of oak species was unaffected by the drought (Roman et al., 2015), there was a small (9.4%) but significant difference ($p < 0.05$) in mean PS of sunlit oak leaves between years (Fig. 3d). This could reflect non-stomatal (i.e. biochemical) limitations to the photosynthetic machinery imposed by the particularly low leaf water potential observed for these species during the drought (Roman et al., 2015). It is worthwhile to note that the decrease in PS of sunlit leaves was somewhat compensated by a significant increase in PS of shaded PS ($p < 0.05$; 21.2%) for oak species (Fig. 3d).

3.2. Leaf-scale spectral indices

Contrary to expectation, scaled PRI (sPRI) values of sunlit and shaded leaves did not show any consistent patterns between dry and wet years (Fig. 3), and the correlation analyses with the leaf PS measurements did not show any significant results at tree and species levels. The sPRI values of the sunlit leaves were generally lower compared to those of the shaded leaves in both years, which may effectively represent higher LUE in shaded portion of canopy. The mean sPRI values of the sunlit leaves (except for sassafras) were generally lower in 2012 (dry) than in 2013 (wet), while those of the shaded leaves were generally higher in 2012 (except for tulip poplar) (Fig. 3). The sPRI values showed more interannual variability for the three isohydric species, while they were not significantly different for two oak species (Fig. 3d). These contrasting patterns between isohydric and anisohydric species led to the difference in the sunlit-to-shaded PRI ratios between dry and wet years (Fig. 4). For all three isohydric species, the mean sPRI ratios ($sPRI_{sunlit}/sPRI_{shaded}$) were significantly lower in 2012 ($p < 0.05$), while not for the two oak species ($p > 0.05$). This demonstrates that the decreases in sPRI were much greater for sunlit than for shaded leaves during the drought, consistent with the leaf-level PS measurements (Fig. 3).

For the other spectral indices (NDVI, $NDVI_{705}$, and EVI), only EVI showed consistently and statistically lower mean values in 2012 for both sunlit and shaded leaves, compared to 2013 (except for the sunlit leaves of sassafras; Fig. S5). $NDVI_{705}$ showed slightly better performance to capture the drought effect and isohydric/anisohydric behavior than NDVI, but these patterns were still not consistent. All three spectral indices did not show any distinct inter-annual differences between the oak species and others, including their sunlit-to-shaded ratios (Fig. S6). Thus all three of the greenness spectral indices failed to capture isohydric vs. anisohydric behavior under the drought condition, supporting that there is no clear evidence that drought-induced changes in leaf PS has any direct implications on these three spectral indices.

3.3. Canopy-scale spectral indices

The canopy-scale NDVI and EVI values showed clear differences between 2012 (dry) and 2013 (wet) years during the peak drought season (July–August) (Fig. 5). Although both vegetation indices show little interannual variability in their maximum values for the period from 2001 to 2014, the mean NDVI and EVI values (July–August) were 5% and 11% less, respectively, in 2012 compared to the mean for 2001–2014 (except 2012). Since leaf NDVI was largely unaffected by drought (Fig. S5) and the decrease in canopy NDVI roughly corresponded with the observed decrease in LAI values (about 5–10%) (Fig. 5c), the changes in canopy structure appear to account for much of the change in NDVI during the drought. On the other hand, canopy EVI declined slightly more during the drought than did NDVI, indicating that both canopy structural and leaf spectral changes were factors in the change in canopy EVI. However, note that decreases in both NDVI and EVI values were substantially smaller than the changes in GEP and NEE values during the drought period (Fig. 1).

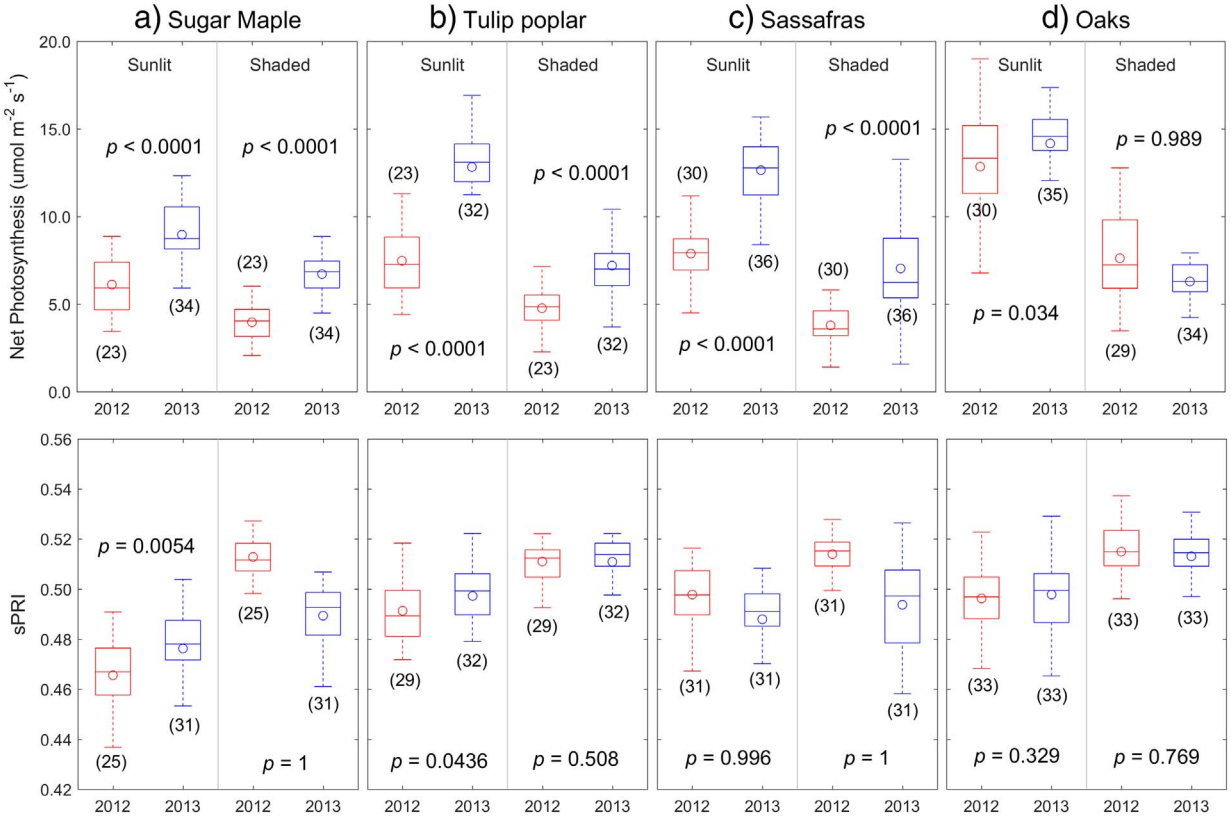

Fig. 3. Boxplots for the measured leaf net photosynthesis (μmol m^{-2} s^{-1}) and sPRI values (dimensionless) from July to August in 2012 (drought year - red) and 2013 (wet year - blue) for three isohydric species: (a) sugar maple, (b) tulip poplar, (c) sassafras, and (d) two anisohydric oaks (two white oaks and one red oak). Leaf reflectance and photosynthesis were measured weekly around midday (10 am–3 pm) for sunlit and shaded leaves separately (Figs. S3 and S4). All measurements represent the tree-level observations from three trees in each group (n = 12 total), which are actually the averaged values from five leaf samples from each tree. The numbers in the parentheses are the total number of tree-level observations, and circles are the mean values. The p-values were from the two-sample t-test with a null hypothesis that the group mean of 2012 is greater than that of 2013. (For interpretation of the references to color in this figure legend, the reader is referred to the web version of this article.)

Similar to the leaf-scale measurements, the pixel-level MODIS sPRI values during the peak drought period (July–August) did not show consistent or statistically different patterns between dry and wet years for both Terra and Aqua images (Fig. 6). The MODIS sPRI values were generally higher than the field observations, possibly due to the difference in the reference band. However, the sPRI values from backward direction images were significantly lower than forward ones in 2012 for both Terra and Aqua images ($p < 0.1$) (Fig. 6). This demonstrates that the decreases in sPRI were much greater in the sunlit portion of the canopy than in shaded portions during the peak drought, consistent with the leaf-level spectral and PS measurements (Figs. 3 and 4). As a result, the backward-to-forward sPRI ratios were consistently lower during the peak drought period (July–August) in 2012 than those in the normal and wet years (Fig. 7). This was similar to the lower sunlit-to-shade sPRI ratios at the leaf scale in 2012 (Fig. 4), although the absolute ratio values are slightly higher at the canopy scale. Given the < 10% basal area composition of the anisohydric species in the study site, it is possible that the leaf-level PRI signal of the isohydric species should be visible at the MODIS pixel scale. However, note that the seasonal drought patterns were more obvious in the Aqua data (local overpass time of approximately 1:30 pm; Fig. 7b) than in Terra data (10:30 am; Fig. 7a), which more resemble GEP and NEE patterns in 2012 and 2013 (Fig. 1). Additionally, these ratios generally remained higher in 2013 (wet), compared to those at the same time in the other two years.

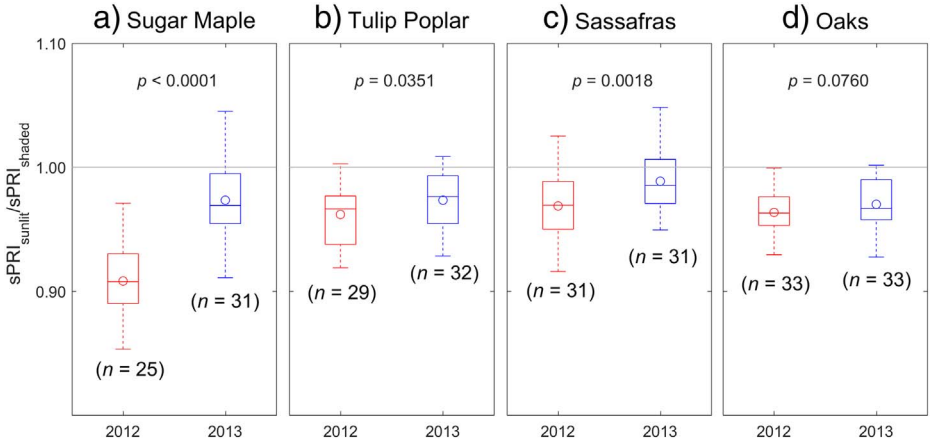

Fig. 4. Boxplots for the sunlit-to-shaded sPRI ratios (dimensionless) from July to August in 2012 (drought year - red) and 2013 (wet year - blue) for three isohydric species: (a) sugar maple, (b) tulip poplar, (c) sassafras, and (d) anisohydric oak species (two white oaks and one red oak). All measurements represent the tree-level observations from three trees in each group, calculated from five sunlit and five shaded leaves from each tree. The numbers in the parentheses are the total number of tree-level observations, and circles show the mean values. The p-values were from the two-sample t-test with a null hypothesis that the group mean of 2012 is greater than that of 2013. (For interpretation of the references to color in this figure legend, the reader is referred to the web version of this article.)

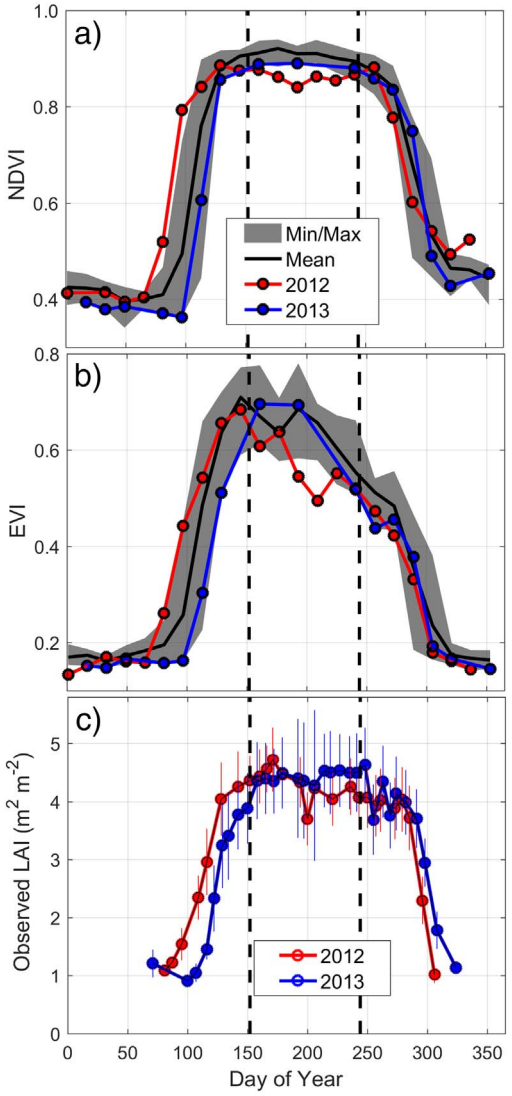

Fig. 5. Seasonal patterns of MODIS (a) NDVI and (b) EVI (MOD13Q1), (c) observed LAI (leaf are index) in 2012 (dry) and 2013 (wet) years. The gray regions represent the minimum and maximum ranges of NDVI and EVI values from 2001 to 2015, except for 2012. LAI values were measured weekly along the three transects around the flux tower (n = 30 total), and the vertical lines represent the standard deviations. The vertical dashed lines show the peak growing season (June–August) of the year.

4. Discussion and conclusions

In this study, we examined the capability of four spectral indices to capture peak drought signals and isohydric/anisohydric behavior at both leaf and canopy scales in the closed deciduous broadleaf forest. NDVI and $NDVI_{705}$ failed to capture the drought signal or the divergent isohydric/anisohydric behavior at the leaf scale, while NDVI did show the canopy-scale structural changes (e.g. LAI) caused by the drought. EVI successfully captured the drought signals at both leaf and canopy scales, but failed to capture the isohydric/anisohydric behavior. Finally, PRI captured both drought signals and divergent isohydric/anisohydric behavior at both leaf and canopy scales once normalized between sunlit (backward direction) and shaded (forward direction) portions of canopy. Consistent with previous literature (e.g. Cheng et al., 2012; Hall et al., 2008), our results showed the directional responses of PRI were larger when drought stress and subsequent photosynthetic down-regulation were greater in the sunlit portion of canopy. It is worthwhile to note that the seasonal drought signals in backward/forward PRI ratios from the MODIS Aqua data were more similar to GEP, NEE, and soil moisture patterns than those from Terra data.

Although PRI captures instantaneous energy dissipations in the xanthophyll cycle, it can be also influenced by seasonal and interannual changes including carotenoid-to-chlorophyll pigment ratios (Filella et al., 2009; Sims et al., 2006; Wong and Gamon, 2015) and sun-target-sensor geometry (Gamon and Bond, 2013). It is also well-known that trees retranslocate their leaf nitrogen under severe drought conditions (Heckathorn and DeLucia, 1994), which might also affect the inter-annual LUE and PRI values between wet and dry years (Garbulsky et al., 2011). Therefore, seasonal and interannual variability of PRIs can be readily confounded by multiple environmental factors, which makes it difficult to detect and standardize drought stress using PRIs (Soudani et al., 2014; Zarco-Tejada et al., 2013; Zhang et al., 2016). Although there were the significant interannual changes in carbon uptakes both at the leaf and canopy scales, we also did not see any consistent shifts or apparent trends in the PRI values between wet and dry years. Likewise, we could not find any significant correlations between the PRI values and the leaf PS measurements both at tree and species levels. However, once normalized using sunlit-to-shade (leaf scale) and backward-to-forward image (canopy scale) ratios under the assumption of increasing the degree of down-regulation during droughts, we could successfully capture the drought effect on divergent behaviors between wet and dry years, between isohydric and anisohydric tree species, and possibly between morning (Terra) and afternoon (Aqua) MODIS images.

Our analysis also agrees well with a recent study by Vicca et al. (2016), who reported that only EVI is capable of detecting drought signals at Hesse Forest in the northeastern France (also a deciduous forest), while PRI and NDVI values did not capture the interannual changes in GPP caused by drought. EVI was originally designed to reduce the spectral variances driven by atmospheric aerosols by including the blue band (Huete et al., 2002). However, it is also sensitive to carotenoid contents, which have high absorption between 400 and 500 nm (Sims and Gamon, 2002) and usually increases during droughts (Liu et al., 2011). However, EVI failed to capture divergent isohydric vs. anisohydric behavior upon drought stress, clearly manifested in the leaf-level PS measurements. Therefore, it is likely that the reduction of EVI during the drought period was driven not by emergent differences in photosynthetic activities, but by the accompanying leaf physiological changes as well as the structural changes at the canopy level, as suggested by Vicca et al. (2016).

Recently, two normalization methods for PRI were proposed by Zarco-Tejada et al. (2013) and Soudani et al. (2014) at different time scales. Zarco-Tejada et al. (2013) used both renormalized difference vegetation and red edge ratio indices to normalize PRI with the drought-induced changes in chlorophyll content and vegetation structure at diurnal scale. Soudani et al. (2014) proposed the correction of PRI values using intercepts of the linear regressions between APAR and PRI (called PRI_0) at seasonal scale. Our normalization method intended to detect species-level responses to severe droughts (isohydricity vs. anisohydricity) for closed deciduous forests, where traditional spectral indices often have limited capability to capture drought-induced structural and/or chlorophyll-related changes due to saturation problems (e.g. Daughtry et al., 2000). Additionally, we reported the divergence of PRI values between sunlit and shaded canopy portions consistently across leaf, canopy, and species levels, which would provide a unique advantage in upscaling drought effect on ecosystem carbon sequestration using spectral remote sensing information. However, the suggested method using backward and forward direction images may not be suitable for sparse forests. It is simply because this method explicitly assumes mutual shadowing between trees (viewing and illumination shadows on vegetative surfaces) are dominant factors controlling canopy bidirectional reflectance distribution function (BRDF) (Li and Strahler, 1992; Li et al., 1995).

Although the divergence in MODIS PRI values between backward (sunlit) and forward (shaded) direction images were found in both Terra and Aqua data, the drought pattern in the sPRI ratios were more

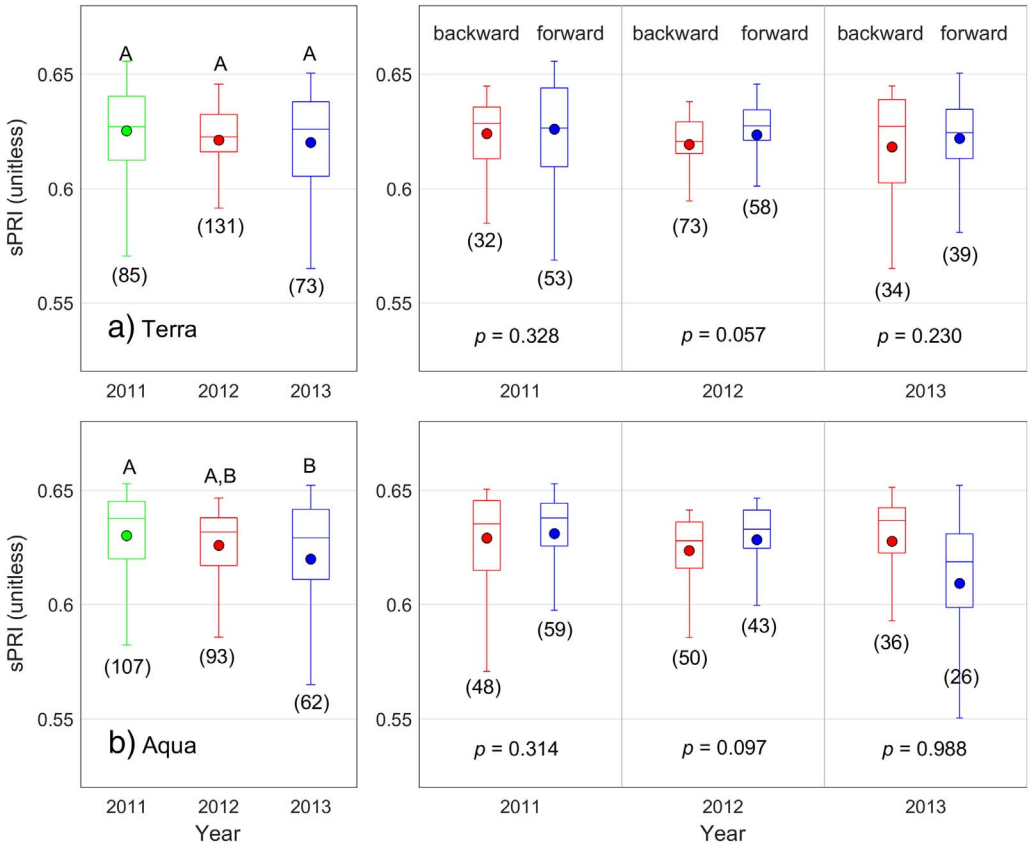

Fig. 6. All sPRI values obtained from MODIS (a) Terra and (b) Aqua data from July through August in normal (2011 – green), dry (2012 – red), and wet (2013 – blue) years. Bar graphs in the right column show the pixel-level PRI values from the backward (red) and forward (blue) direction MODIS images each year. Backward direction images include more sunlit portion of the canopy, while forward direction images include more shaded portion. The numbers in the parentheses are the total number of pixel-level MODIS PRI values used in the study (Fig. S7), and circles show the mean values. Different letters (A–B) denote significant differences in the group means using an analysis of variance (ANOVA) test ($p < 0.05$). The p-values were from the two-sample t-test with a null hypothesis that the group mean of 2012 is greater than that of 2013. (For interpretation of the references to color in this figure legend, the reader is referred to the web version of this article.)

obvious in the Aqua data, compared to the Terra. There are two possible explanations for this. First, it might be mainly due to calibration issues of Terra by the problem in the solar diffuser door (e.g. Franz et al., 2008), which affects more the shorter wavelength bands. This issue was expected to be improved in the MODIS Collection 6, but it is quite possible that it did not completely remove the problems identified in the Collection 5 (Wu et al., 2013). Note that Gamon et al. (2016) also only used Aqua data to calculate CCI to monitor evergreen photosynthetic activity. Second, the drought stress and subsequent photosynthetic downregulation are likely to be greater in the afternoon rather than in the morning (Sims et al., 2005). The hourly LUE values from the flux tower also usually showed strong diurnal patterns especially in the non-cloudy days (Fig. S8). These LUE values and their variances are often higher in the morning and lower in the afternoon, which might make drought signals unclear for the Terra data.

Many coupled modeling efforts have shown that separate modeling between sunlit and shaded portions of canopy was the most efficient way to simulate daily photosynthesis without multilayer simulations (Chen et al., 1999; de Pury and Farquhar, 1997; Song et al., 2009; Wang and Leuning, 1998). The dynamic separation between sunlit and shaded leaves is also justified in that the upper sunlit canopy is usually light saturated (lower LUE), and therefore more vulnerable to drought stress, while the lower shaded canopy responds linearly to irradiance with higher LUE (de Pury and Farquhar, 1997; Wang and Leuning, 1998). This vertical transition of rate determining factors for photosynthesis typically led to the distributions of leaf biochemical and structural traits along canopy depth profile, such as carbon-to-nitrogen ratios and specific leaf area (Field, 1983; de Pury and Farquhar, 1997). Recently, Coops et al. (2017) also showed that incorporating vertical gradients of PRI-derived LUE is critical in upscaling leaf-scale physiological behavior into canopy-level GPP in the closed deciduous canopy. However, to date few remote sensing based global GPP models incorporate two-leaf modeling structures because of computational efficiency (Zhou et al., 2016). In this study, we suggest that it would be critical to incorporate the two-leaf model structure to properly simulate the drought effect on ecosystem carbon sequestrations under climate change considering emergent divergence between sunlit and shade portions of canopy.

Parameterizing water use strategies into terrestrial ecosystem models will essentially require mapping the distribution of anisohydric and isohydric trees across the different spatial scales. However, mapping isohydricity from the parameter space along the isohydric/anisohydric continuum to landscape space requires very detailed vegetation information with intensive field observations during drought (Meinzer et al., 2016). To date, we are aware of only one attempt to develop a map of the distribution of isohydricity across the landscape (Konings and Gentine, 2016). That work relied on remotely-sensed observations of vegetation optical depth using Advanced Microwave Scanning Radiometer-E (AMSR-E) data, which has been previously shown to be correlated with leaf water potential. Our approach suggests another path forward for using emergent spectral signatures during droughts to map the distribution of isohydric and anisohydric species. This study presents a theoretical framework for large-scale isohydricity mapping based on emergent spectral signatures under drought stress using multi-angle MODIS images. This direct mapping of ecosystem sensitivity to drought stress may represent a significant step forward from the simplistic drought scalars currently used in remote-sensing based productivity models.

5. Conclusions

In this study, we examined the capability of four spectral indices to capture peak drought signals and isohydric/anisohydric behavior in a deciduous broadleaf forest using in-situ spectral measurements and multi-angle remote sensing images. After normalizing between sunlit (backward) and shaded (forward) portions of canopy, PRI successfully captured both drought signals and species-level drought responses at both leaf and canopy scales. Drought stress and subsequent photosynthetic downregulation were greater in the sunlit portion of canopy,

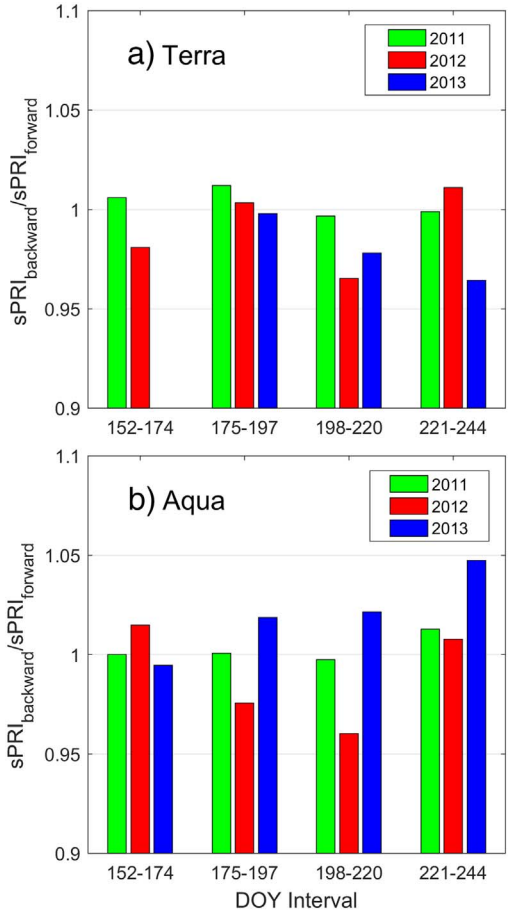

Fig. 7. The sPRI ratios of backward to forward direction images for MODIS (a) Terra and (b) Aqua data from June through August in normal (2011 – green), dry (2012 – red), and wet (2013 – blue) years in the study site. The definition of backward and forward direction MODIS images are provided in Eq. (3). The sPRI ratios were calculated roughly at three-week intervals from the group means of the pixel-level MODIS PRI values at each day of year (DOY) interval (Fig. S7). (For interpretation of the references to color in this figure legend, the reader is referred to the web version of this article.)

which provides us a key to capture species- and canopy-level drought responses in the study site. Importantly, this work may represent a significant step forward in our ability to dynamically predict the impact of water stress on forest carbon gain by providing a theoretical framework for mapping large-scale isohydricity based on emergent spectral responses under drought stress.

Acknowledgements

This research was supported by NASA Carbon Science program (Grant # NNX17AE69G) to Drs. T Hwang and K Novick. Funding for the leaf-scale PS and spectral measurements was provided by the NASA Terrestrial Ecology program (Grant # NNX10AF40G) to Drs. A.F. Rahman and D.A. Sims. Funding for the Morgan Monroe Flux Tower is provided by the AmeriFlux Management Project, administered by Lawrence Berkeley National Lab with support from the US Department of Energy. We thank to three anonymous reviewers for their comments and supports. We also thank to Steve Scott, Bo Stearman, and Rob Conover for help in collection of field data.

Appendix A. Supplementary data

Supplementary data to this article can be found online at http://dx.doi.org/10.1016/j.rse.2017.07.033.

References

Adams, H.D., Guardiola-Claramonte, M., Barron-Gafford, G.A., Villegas, J.C., Breshears, D.D., Zou, C.B., Troch, P.A., Huxman, T.E., 2009. Temperature sensitivity of drought-induced tree mortality portends increased regional die-off under global-change-type drought. Proc. Natl. Acad. Sci. 106, 7063–7066.

Allen, C.D., Breshears, D.D., 2007. Climate-induced forest dieback as an emergent global phenomenon. Eos. Trans. AGU 88, 504.

Asner, G.P., Nepstad, D., Cardinot, G., Ray, D., 2004. Drought stress and carbon uptake in an Amazon forest measured with spaceborne imaging spectroscopy. Proc. Natl. Acad. Sci. U. S. A. 101, 6039–6044.

Barton, C.V.M., North, P., 2001. Remote sensing of canopy light use efficiency using the photochemical reflectance index: model and sensitivity analysis. Remote Sens. Environ. 78, 264–273.

Brzostek, E.R., Dragoni, D., Schmid, H.P., Rahman, A.F., Sims, D., Wayson, C.A., Johnson, D.J., Phillips, R.P., 2014. Chronic water stress reduces tree growth and the carbon sink of deciduous hardwood forests. Glob. Chang. Biol. 20, 2531–2539.

Chen, J.M., Liu, J., Cihlar, J., Goulden, M.L., 1999. Daily canopy photosynthesis model through temporal and spatial scaling for remote sensing applications. Ecol. Model. 124, 99–119.

Cheng, Y.-B., Middleton, E.M., Zhang, Q., Corp, L.A., Dandois, J., Kustas, W.P., 2012. The photochemical reflectance index from directional cornfield reflectances: observations and simulations. Remote Sens. Environ. 124, 444–453.

Choat, B., Jansen, S., Brodribb, T.J., Cochard, H., Delzon, S., Bhaskar, R., Bucci, S.J., Feild, T.S., Gleason, S.M., Hacke, U.G., Jacobsen, A.L., Lens, F., Maherali, H., Martinez-Vilalta, J., Mayr, S., Mencuccini, M., Mitchell, P.J., Nardini, A., Pittermann, J., Pratt, R.B., Sperry, J.S., Westoby, M., Wright, I.J., Zanne, A.E., 2012. Global convergence in the vulnerability of forests to drought. Nature 491, 752–755.

Coops, N.C., Hilker, T., Hall, F.G., Nichol, C.J., Drolet, G.G., 2010. Estimation of light-use efficiency of terrestrial ecosystems from space: a status report. Bioscience 60, 788–797.

Coops, N.C., Hermosilla, T., Hilker, T., Black, T.A., 2017. Linking stand architecture with canopy reflectance to estimate vertical patterns of light-use efficiency. Remote Sens. Environ. 194, 322–330.

Dai, A., 2013. Increasing drought under global warming in observations and models. Nat. Clim. Chang. 3, 52–58.

Daughtry, C., Walthall, C., Kim, M., De Colstoun, E.B., McMurtrey, J., 2000. Estimating corn leaf chlorophyll concentration from leaf and canopy reflectance. Remote Sens. Environ. 74, 229–239.

de Pury, D.G.G., Farquhar, G.D., 1997. Simple scaling of photosynthesis from leaves to canopies without the errors of big-leaf models. Plant Cell Environ. 20, 537–557.

Demmig-Adams, B., Adams III, W.W., 1996. Xanthophyll cycle and light stress in nature: uniform response to excess direct sunlight among higher plant species. Planta 198, 460–470.

Didan, K., Huete, A., 2006. MODIS Vegetation Index Product Series Collection 5 Change Summary. TBRS Lab., University of Arizona.

Dragoni, D., Schmid, H.P., Wayson, C.A., Potter, H., Grimmond, C.S.B., Randolph, J.C., 2011. Evidence of increased net ecosystem productivity associated with a longer vegetated season in a deciduous forest in south-central Indiana, USA. Glob. Chang. Biol. 17, 886–897.

Drolet, G.G., Huemmrich, K.F., Hall, F.G., Middleton, E.M., Black, T.A., Barr, A.G., Margolis, H.A., 2005. A MODIS-derived photochemical reflectance index to detect inter-annual variations in the photosynthetic light-use efficiency of a boreal deciduous forest. Remote Sens. Environ. 98, 212–224.

Drolet, G., Middleton, E., Huemmrich, K., Hall, F., Amiro, B., Barr, A., Black, T., McCaughey, J., Margolis, H., 2008. Regional mapping of gross light-use efficiency using MODIS spectral indices. Remote Sens. Environ. 112, 3064–3078.

Ehman, J., Schmid, H., Grimmond, C., Randolph, J., Hanson, P., Wayson, C., Cropley, F., 2002. An initial intercomparison of micrometeorological and ecological inventory estimates of carbon exchange in a mid-latitude deciduous forest. Glob. Chang. Biol. 8, 575–589.

Field, C., 1983. Allocating leaf nitrogen for the maximization of carbon gain: leaf age as a control on the allocation program. Oecologia 56, 341–347.

Filella, I., Porcar-Castell, A., Munné-Bosch, S., Bäck, J., Garbulsky, M.F., Peñuelas, J., 2009. PRI assessment of long-term changes in carotenoids/chlorophyll ratio and short-term changes in de-epoxidation state of the xanthophyll cycle. Int. J. Remote Sens. 30, 4443–4455.

Ford, C.R., Hubbard, R.M., Vose, J.M., 2011. Quantifying structural and physiological controls on variation in canopy transpiration among planted pine and hardwood species in the southern Appalachians. Ecohydrology 4, 183–195.

Franz, B.A., Kwiatowska, E.J., Meister, G., McClain, C.R., 2008. Moderate resolution imaging spectroradiometer on Terra: limitations for ocean color applications. J. Appl. Remote. Sens. 2, 023525.

Gamon, J.A., Bond, B., 2013. Effects of irradiance and photosynthetic downregulation on the photochemical reflectance index in Douglas-fir and ponderosa pine. Remote Sens. Environ. 135, 141–149.

Gamon, J., Penuelas, J., Field, C., 1992. A narrow-waveband spectral index that tracks diurnal changes in photosynthetic efficiency. Remote Sens. Environ. 41, 35–44.

Gamon, J., Serrano, L., Surfus, J., 1997. The photochemical reflectance index: an optical indicator of photosynthetic radiation use efficiency across species, functional types, and nutrient levels. Oecologia 112, 492–501.

Gamon, J.A., Huemmrich, K.F., Wong, C.Y., Ensminger, I., Garrity, S., Hollinger, D.Y., Noormets, A., Penuelas, J., 2016. A remotely sensed pigment index reveals photosynthetic phenology in evergreen conifers. Proc. Natl. Acad. Sci. U. S. A. 113, 13087–13092.

Garbulsky, M.F., Peñuelas, J., Gamon, J., Inoue, Y., Filella, I., 2011. The photochemical reflectance index (PRI) and the remote sensing of leaf, canopy and ecosystem radiation use efficiencies: a review and meta-analysis. Remote Sens. Environ. 115, 281–297.
Garbulsky, M.F., Peñuelas, J., Ogaya, R., Filella, I., 2013. Leaf and stand-level carbon uptake of a Mediterranean forest estimated using the satellite-derived reflectance indices EVI and PRI. Int. J. Remote Sens. 34, 1282–1296.
Goerner, A., Reichstein, M., Rambal, S., 2009. Tracking seasonal drought effects on ecosystem light use efficiency with satellite-based PRI in a Mediterranean forest. Remote Sens. Environ. 113, 1101–1111.
Goerner, A., Reichstein, M., Tomelleri, E., Hanan, N., Rambal, S., Papale, D., Dragoni, D., Schmullius, C., 2011. Remote sensing of ecosystem light use efficiency with MODIS-based PRI. Biogeosciences 8, 189–202.
Hall, F.G., Hilker, T., Coops, N.C., Lyapustin, A., Huemmrich, K.F., Middleton, E., Margolis, H., Drolet, G., Black, T.A., 2008. Multi-angle remote sensing of forest light use efficiency by observing PRI variation with canopy shadow fraction. Remote Sens. Environ. 112, 3201–3211.
Hall, F.G., Hilker, T., Coops, N.C., 2012. Data assimilation of photosynthetic light-use efficiency using multi-angular satellite data: I. Model formulation. Remote Sens. Environ. 121, 301–308.
He, M., Kimball, J.S., Running, S., Ballantyne, A., Guan, K., Huemmrich, F., 2016. Satellite detection of soil moisture related water stress impacts on ecosystem productivity using the MODIS-based photochemical reflectance index. Remote Sens. Environ. 186, 173–183.
Heckathorn, S.A., DeLucia, E.H., 1994. Drought-induced nitrogen retranslocation in perennial C4 grasses of tallgrass prairie. Ecology 75, 1877–1886.
Hilker, T., Coops, N.C., Hall, F.G., Black, T.A., Wulder, M.A., Nesic, Z., Krishnan, P., 2008. Separating physiologically and directionally induced changes in PRI using BRDF models. Remote Sens. Environ. 112, 2777–2788.
Huete, A.R., Liu, H.Q., Batchily, K., vanLeeuwen, W., 1997. A comparison of vegetation indices global set of TM images for EOS-MODIS. Remote Sens. Environ. 59, 440–451.
Huete, A., Didan, K., Miura, T., Rodriguez, E.P., Gao, X., Ferreira, L.G., 2002. Overview of the radiometric and biophysical performance of the MODIS vegetation indices. Remote Sens. Environ. 83, 195–213.
Hwang, T., Kang, S., Kim, J., Kim, Y., Lee, D., Band, L., 2008. Evaluating drought effect on MODIS Gross Primary Production (GPP) with an eco-hydrological model in the mountainous forest, East Asia. Glob. Chang. Biol. 14, 1037–1056.
Klein, T., Yakir, D., Buchmann, N., Gruenzweig, J.M., 2014. Towards an advanced assessment of the hydrological vulnerability of forests to climate change-induced drought. New Phytol. 201, 712–716.
Konings, A.G., Gentine, P., 2017. Global variations in ecosystem-scale isohydricity. Glob. Chang. Biol. 23, 891–905.
Li, X., Strahler, A.H., 1992. Geometric-optical bidirectional reflectance modeling of the discrete crown vegetation canopy: effect of crown shape and mutual shadowing. IEEE Trans. Geosci. Remote Sens. 30, 276–292.
Li, X., Strahler, A.H., Woodcock, C.E., 1995. A hybrid geometric optical-radiative transfer approach for modeling albedo and directional reflectance of discontinuous canopies. IEEE Trans. Geosci. Remote Sens. 33, 466–480.
Liu, C., Liu, Y., Guo, K., Fan, D., Li, G., Zheng, Y., Yu, L., Yang, R., 2011. Effect of drought on pigments, osmotic adjustment and antioxidant enzymes in six woody plant species in karst habitats of southwestern China. Environ. Exp. Bot. 71, 174–183.
Marchin, R., Zeng, H., Hoffmann, W., 2010. Drought-deciduous behavior reduces nutrient losses from temperate deciduous trees under severe drought. Oecologia 163, 845–854.
Martinez-Vilalta, J., Poyatos, R., Aguade, D., Retana, J., Mencuccini, M., 2014. A new look at water transport regulation in plants. New Phytol. 204, 105–115.
Matheny, A.M., Fiorella, R.P., Bohrer, G., Poulsen, C.J., Morin, T.H., Wunderlich, A., Vogel, C.S., Curtis, P.S., 2017. Contrasting strategies of hydraulic control in two codominant temperate tree species. Ecohydrology 10, 1–16.
McDowell, N.G., Allen, C.D., 2015. Darcy's law predicts widespread forest mortality under climate warming. Nat. Clim. Chang. 5, 669–672.
McDowell, N., Pockman, W.T., Allen, C.D., Breshears, D.D., Cobb, N., Kolb, T., Plaut, J., Sperry, J., West, A., Williams, D.G., Yepez, E.A., 2008. Mechanisms of plant survival and mortality during drought: why do some plants survive while others succumb to drought? New Phytol. 178, 719–739.
Meinzer, F.C., Woodruff, D.R., Marias, D.E., Smith, D.D., McCulloh, K.A., Howard, A.R., Magedman, A.L., 2016. Mapping 'hydroscapes' along the iso- to anisohydric continuum of stomatal regulation of plant water status. Ecol. Lett. 19, 1343–1352.
Meinzer, F.C., Smith, D.D., Woodruff, D.R., Marias, D.E., McCulloh, K.A., Howard, A.R., Magedman, A.L., 2017. Stomatal kinetics and photosynthetic gas exchange along a continuum of iso-to anisohydric regulation of plant water status. Plant Cell Environ.
Munne-Bosch, S., Jubany-Mari, T., Alegre, L., 2001. Drought-induced senescence is characterized by a loss of antioxidant defences in chloroplasts. Plant Cell Environ. 24, 1319–1327.
Novick, K.A., Oishi, A.C., Ward, E.J., Siqueira, M.B., Juang, J.Y., Stoy, P.C., 2015. On the difference in the net ecosystem exchange of CO_2 between deciduous and evergreen forests in the southeastern United States. Glob. Chang. Biol. 21, 827–842.
Novick, K.A., Miniat, C.F., Vose, J.M., 2016. Drought limitations to leaf-level gas exchange: results from a model linking stomatal optimization and cohesion-tension theory. Plant Cell Environ. 39, 583–596.
O'Gorman, P.A., Schneider, T., 2009. The physical basis for increases in precipitation extremes in simulations of 21st-century climate change. Proc. Natl. Acad. Sci. U. S. A. 106, 14773–14777.
Penuelas, J., Filella, I., Gamon, J.A., 1995. Assessment of photosynthetic radiation-use efficiency with spectral reflectance. New Phytol. 131, 291–296.
Rahman, A., Cordova, V., Gamon, J., Schmid, H., Sims, D., 2004. Potential of MODIS ocean bands for estimating CO_2 flux from terrestrial vegetation: a novel approach. Geophys. Res. Lett. 31.
Roman, D., Novick, K., Brzostek, E., Dragoni, D., Rahman, F., Phillips, R., 2015. The role of isohydric and anisohydric species in determining ecosystem-scale response to severe drought. Oecologia 179, 641–654.
Schmid, H.P., Grimmond, C.S.B., Cropley, F., Offerle, B., Su, H.-B., 2000. Measurements of CO_2 and energy fluxes over a mixed hardwood forest in the mid-western United States. Agric. For. Meteorol. 103, 357–374.
Seager, R., Tzanova, A., Nakamura, J., 2009. Drought in the Southeastern United States: Causes, Variability over the Last Millennium, and the Potential for Future Hydroclimate Change. J. Clim. 22, 5021–5045.
Sims, D.A., Gamon, J.A., 2002. Relationships between leaf pigment content and spectral reflectance across a wide range of species, leaf structures and developmental stages. Remote Sens. Environ. 81, 337–354.
Sims, D.A., Rahman, A.F., Cordova, V.D., Baldocchi, D.D., Flanagan, L.B., Goldstein, A.H., Hollinger, D.Y., Misson, L., Monson, R.K., Schmid, H.P., 2005. Midday values of gross CO_2 flux and light use efficiency during satellite overpasses can be used to directly estimate eight-day mean flux. Agric. For. Meteorol. 131, 1–12.
Sims, D.A., Luo, H., Hastings, S., Oechel, W.C., Rahman, A.F., Gamon, J.A., 2006. Parallel adjustments in vegetation greenness and ecosystem CO_2 exchange in response to drought in a Southern California chaparral ecosystem. Remote Sens. Environ. 103, 289–303.
Sims, D.A., Brzostek, E.R., Rahman, A.F., Dragoni, D., Phillips, R.P., 2014. An improved approach for remotely sensing water stress impacts on forest C uptake. Glob. Chang. Biol. 20, 2856–2866.
Song, C.H., Katul, G., Oren, R., Band, L.E., Tague, C.L., Stoy, P.C., McCarthy, H.R., 2009. Energy, water, and carbon fluxes in a loblolly pine stand: results from uniform and gappy canopy models with comparisons to eddy flux data. J. Geophys. Res. Biogeosci. 114, G04021.
Song, C., Dannenberg, M.P., Hwang, T., 2013. Optical remote sensing of terrestrial ecosystem primary productivity. Prog. Phys. Geogr. 37, 834–854.
Soudani, K., Hmimina, G., Dufrêne, E., Berveiller, D., Delpierre, N., Ourcival, J.-M., Rambal, S., Joffre, R., 2014. Relationships between photochemical reflectance index and light-use efficiency in deciduous and evergreen broadleaf forests. Remote Sens. Environ. 144, 73–84.
Sperry, J.S., Wang, Y., Wolfe, B.T., Mackay, D.S., Anderegg, W.R., McDowell, N.G., Pockman, W.T., 2016. Pragmatic hydraulic theory predicts stomatal responses to climatic water deficits. New Phytol. 212, 577–589.
Stoy, P.C., Katul, G.G., Siqueira, M.B.S., Juang, J.-Y., Novick, K.A., McCarthy, H.R., Oishi, A.C., Uebelherr, J.M., Kim, H.-S., Oren, R., 2006. Separating the effects of climate and vegetation on evapotranspiration along a successional chronosequence in the southeastern US. Glob. Chang. Biol. 12, 2115–2135.
Suárez, L., Zarco-Tejada, P.J., Sepulcre-Cantó, G., Pérez-Priego, O., Miller, J.R., Jiménez-Muñoz, J., Sobrino, J., 2008. Assessing canopy PRI for water stress detection with diurnal airborne imagery. Remote Sens. Environ. 112, 560–575.
Sulman, B.N., Roman, D.T., Scanlon, T.M., Wang, L., Novick, K.A., 2016. Comparing methods for partitioning a decade of carbon dioxide and water vapor fluxes in a temperate forest. Agric. For. Meteorol. 226, 229–245.
Tucker, C.J., 1979. Red and photographic infrared linear combinations for monitoring vegetation. Remote Sens. Environ. 8, 127–150.
Vicca, S., Balzarolo, M., Filella, I., Granier, A., Herbst, M., Knohl, A., Longdoz, B., Mund, M., Nagy, Z., Pintér, K., 2016. Remotely-sensed detection of effects of extreme droughts on gross primary production. Sci Rep 6.
Wang, Y.-P., Leuning, R., 1998. A two-leaf model for canopy conductance, photosynthesis and partitioning of available energy I: model description and comparison with a multi-layered model. Agric. For. Meteorol. 91, 89–111.
Wong, C.Y., Gamon, J.A., 2015. Three causes of variation in the photochemical reflectance index (PRI) in evergreen conifers. New Phytol. 206, 187–195.
Wu, A., Xiong, X., Doelling, D.R., Morstad, D., Angal, A., Bhatt, R., 2013. Characterization of Terra and Aqua MODIS VIS, NIR, and SWIR spectral bands' calibration stability. IEEE Trans. Geosci. Remote Sens. 51, 4330–4338.
Xu, L., Baldocchi, D.D., 2003. Seasonal trends in photosynthetic parameters and stomatal conductance of blue oak (*Quercus douglasii*) under prolonged summer drought and high temperature. Tree Physiol. 23, 865–877.
Yi, K., Dragoni, D., Phillips, R.P., Roman, D.T., Novick, K.A., 2017. Dynamics of stem water uptake among isohydric and anisohydric species experiencing a severe drought. Tree Physiol. 1–14.
Zarco-Tejada, P.J., González-Dugo, V., Williams, L.E., Suárez, L., Berni, J.A.J., Goldhamer, D., Fereres, E., 2013. A PRI-based water stress index combining structural and chlorophyll effects: assessment using diurnal narrow-band airborne imagery and the CWSI thermal index. Remote Sens. Environ. 138, 38–50.
Zhang, C., Filella, I., Garbulsky, M., Peñuelas, J., 2016. Affecting factors and recent improvements of the photochemical reflectance index (PRI) for remotely sensing foliar, canopy and ecosystemic radiation-use efficiencies. Remote Sens. 8, 677.
Zhao, M., Heinsch, F.A., Nemani, R.R., Running, S.W., 2005. Improvements of the MODIS terrestrial gross and net primary production global data set. Remote Sens. Environ. 95, 164–176.
Zhou, Y., Wu, X., Ju, W., Chen, J.M., Wang, S., Wang, H., Yuan, W., Black, A., Jassal, R., Ibrom, A., 2016. Global parameterization and validation of a two-leaf light use efficiency model for predicting gross primary production across FLUXNET sites. J. Geophys. Res. Biogeosci. 121, 1045–1072.